Mechanical properties and healing efficiency of 3D-printed ABS vascular based self-healing cementitious composite

Experiments and modelling

Wan, Zhi; Xu, Yading; Zhang, Yu; He, Shan; Šavija, Branko

DOI
10.1016/j.engfracmech.2022.108471

Publication date
2022

Document Version
Final published version

Published in
Engineering Fracture Mechanics

Engineering Fracture Mechanics 267 (2022) 108471

Contents lists available at ScienceDirect

Engineering Fracture Mechanics

journal homepage: www.elsevier.com/locate/engfracmech

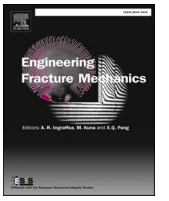

Mechanical properties and healing efficiency of 3D-printed ABS vascular based self-healing cementitious composite: Experiments and modelling

Zhi Wan, Yading Xu *, Yu Zhang, Shan He, Branko Šavija

Faculty of Civil Engineering and Geosciences, Delft University of Technology, 2628CN Delft, the Netherlands

ARTICLE INFO

Keywords:
3D printing
Vascular based self-healing concrete
Printing parameter
Numerical simulation

ABSTRACT

Cracking is one of the main causes for deterioration of concrete structures. Self-healing concrete with 3D-printed vascular networks has excellent potential for autonomous self-healing. This approach is scarcely investigated: no studies have been devoted to the influence of printing parameters on the properties of vascular based self-healing concrete. In this work, three-dimensional vascular structures with complex geometry were designed and printed with 4 different sets of printing parameters. First, the influence of the four, nominally identical, vascular networks on the initial flexural strength of self-healing concretes was experimentally investigated. In parallel, numerical modeling with a concrete damaged plasticity model (CDPM) in Abaqus software is used to simulate the influence of vascular networks on the mechanical properties of the self-healing composite. After the 4-point bending tests, epoxy resin is injected into the vascular networks as the healing agent to seal the cracks. Then, flexural strength regain and watertightness recovery were also measured. Based on the obtained results, we found that vascular based self-healing concretes have lower initial flexural strengths than the reference sample, as expected. The magnitude of the strength drop is shown to depend strongly on the printing parameters: the specimens with horizontally-printed vascular networks have higher flexural strength than the vertically-printed counterparts. Furthermore, vascular networks with a smaller printing layer-height have less influence on the initial flexural strength of vascular-based self-healing concrete compared to those with the larger printing layer-height. In terms of watertightness recovery, all tested vascular based self-healing samples showed a full (100%) recovery, which means that the printing direction and printing layer-height do not have an obvious effect on the watertightness recovery in this study. Numerical simulations of the mechanical performance of the composites with the CDPM show good agreement with the experiments, although printing quality of the vascular network influences the simulation accuracy. These simulations show great potential of using numerical simulations to design vascular based self-healing concrete in order to minimize a drop in mechanical properties, without compromising the healing efficiency. Overall, the designed 3D-printed vascular self-healing concretes show remarkable strength regain and watertightness recovery and provide a good basis for further research.

* Corresponding author.
E-mail address: Y.Xu-5@tudelft.nl (Y. Xu).

https://doi.org/10.1016/j.engfracmech.2022.108471
Received 20 September 2021; Received in revised form 17 March 2022; Accepted 12 April 2022
Available online 18 April 2022

1. Introduction

Crack formation is one of the main causes for deterioration of concrete structures, as harmful liquids or gasses may penetrate into the matrix along these cracks and cause reinforcement corrosion [1,2]. Self-healing concrete is a promising construction material to address this issue due to its capacity of healing the cracks with no or little human intervention [3]. In accordance with approaches originating in the field of self-healing polymers, self-healing in cementitious materials can be broadly classified into intrinsic healing, capsule-based healing and vascular-based healing [4]. Inspired by the fact that blood-vessels enable the rapid and continuous transport of healing materials to the damaged location[5], a vascular network can be similarly designed and embedded in concrete to seal cracks that occur. Compared with the other two approaches, vascular based self-healing has some unique advantages: (1) additional healing agents can be provided if needed, which facilitates repeating of the self-healing process, even if a crack occurs in the same location more than once [6–9]; (2) the maximum healable width of cracks using vascular based self-healing concrete is larger than other self-healing methods due to the availability of sufficient healing agent [10].

According to previous studies [5,11,12], vascular material and vascular structure are of great significance for the healing efficiency of vascular-based self-healing concrete. In terms of vascular material, to facilitate the triggering of the self-healing process and the timely release of the healing agents, the vascular network is usually fabricated with either brittle materials or removable materials. Brittle materials are the most widely-used material for vascular network. Several researchers embedded glass tubes in the cementitious matrix as channels to transport the healing agent [13–15]. However, a problem when using glass tubes may be the alkali–silica reaction induced by the aggressive environment in the concrete, which has adverse effects on the durability of tubes and concrete. Besides, a glass vascular may break during the casting process. Alternatively, others developed the vascular self-healing concrete by building silicone tubes [16], Polyvinyl chloride (PVC) tubes [17], Polyethylene terephthalate (PET) tubes [18] or ceramic tubes [9]. The presence of such materials in concrete may have some unfavorable influences on the self-healing process. For example, the different Elastic moduli between the vascular material and the matrix may cause delamination, which results in reduction of the healing efficiency for not rupturing of vascular networks. Furthermore, in certain cases the organic healing agents may react with the vascular material before healing the crack. To overcome those problems, some researchers used hollow channels to create the vascular network for self-healing purpose. Sangadji and Schlangen [10] used the large pores inherently present in porous network concrete as hollow channels to transport healing agent to cracked region. Davies [1] used heat shrinking tubing or polyurethane tubing to create 2D vascular network in cementitious materials. Except in the field of cementitious materials, similar approaches have also used in self-healing polymers or composites. Patrick [19] formed 3D vascular networks via the vaporization of sacrificial components (VaSC) process in polymers. Boba [20] created a network by placing Nichrome wires coated with polylactic acid between the composite layers. Although hollow channels could benefit the healing process, self-healing concrete without vascular materials tends to be more brittle if no extra reinforcement is embedded.

As to the structure of vascular network, 1-D tubular structure or 2-D planar vascular are commonly-used [1,9,18]. However, the relatively simple structure of vascular networks significantly reduces the self-healing efficiency of current vascular based self-healing concrete. Particularly, when cracks are parallel with the vascular network, the embedded tubes may not rupture timely and the self-healing mechanism will not be triggered. In order to solve those problems, 3D printing technology is introduced to create 3D vascular networks for self-healing purpose [8,19,21]. Compared with other fabrication techniques for vascular networks, 3D printing enables creation of complex vascular networks in self-healing concretes. Similar to the vessel system in animals, vascular networks with different hierarchy in self-healing concretes are expected to be more functional without significantly reducing the initial properties (mechanical strengths or permeability). According to a recent study [22], 3D vascular networks in self-healing concrete show a better healing efficiency and strength recovery compared with 1-D or 2-D vascular networks. In previous studies, most researchers attached importance on the influence of printing materials or healing agents on the healing efficiency, while disregarding the effect of printing parameters on the vascular based self-healing concrete. It should be noted that common 3D printing techniques, such as fused filament deposition (FFD), are layer-by-layer processes, and result in anisotropy of the material properties and imperfections (voids, pores) on different length scales, depending on the printing parameters [23]. This may have an impact on the healing efficiency as well as the mechanical properties of the concrete with vascular networks, when non-dissolvable materials are used for printing. The adverse influence of the embedded vascular networks on the initial properties of self-healing concrete should be minimized.

As to the design of vascular networks for self-healing, there are mainly three approaches. Early pioneers qualitatively design the vascular network based on biological systems. For example, White et al[24] designed the vascular according to the capillary network in the dermis of skin. Schlangen [10] created the porous network concrete for self-healing inspired by the bone morphology. Besides, flow-efficiency is taken as the main metric to design vascular. The fluidity of different structures networks are compared based on experimental results. Wang [25] investigated the flow behavior of grid structure and tree structure. Li [22] designed a 3D-vascular network based on Murray's law and compared the properties of self-healing concretes with 1-D/2-D/3-D vascular networks. In other research [26], instead of only focusing on fluid flow, multiple requirements are considered during vascular design when using evolutionary algorithms such as Genetic algorithm (GA). It is obvious that these designing approaches heavily rely on experiments and it is often time-consuming and significant resources are utilized. Compared with traditional methods, machine learning (ML) is a promising way for design work. Currently, ML is widely used in design of mechanical materials for its capacity of discovering the complicated relation from input to output [27]. Gu [28] designed composite materials with better quality using ML. Similarly, ML could be also used for the design for vascular network in self-healing concretes. However, ML is data-hungry and it is essential to generate a reliable dataset before designing the vascular network.

Therefore, in this work, we carry out a feasibility study of using numerical models to simulate the mechanical response of 3D-printed vascular based self-healing concretes. In addition, an in-depth investigation on the influence of printing parameters on the

strength regain and watertightness recovery of vascular self-healing concrete was carried out. In particular, an octet-structural vascular network was designed and printed using different printing parameters. Concrete damaged plasticity model (CDPM) was employed to simulate 4-point bending tests loaded with a constant crack opening speed. The simulation results are compared with the experiments. Subsequently, epoxy resin was injected as the healing agent to heal the cracks via the embedded vascular networks. The strength regain and watertightness recovery of the four vascular based self-healing concretes was compared to study the influence of printing parameters. Finally, the strength recovery potential of the four vascular based self-healing concretes was investigated by analyzing the flexural strength before and after 2 healing processes. Note that, considering that the measurement of crack width becomes inaccurate because the healed specimens can undergo large deflections, their flexural strength was obtained by 4-point bending test controlled by a constant vertical displacement speed instead of a constant crack opening speed, as done in the case of virgin specimens.

2. Experiments

2.1. Fabrication of 3D-printed vascular networks

To improve the healing efficiency and enable multiple healing process for vascular self-healing concrete, an octet-structure lattice is designed as the vascular network for delivering the healing agent to the crack regions. For the designed vascular, there are 4 or 8 connecting paths for each node. The added redundancy allows healing agents to reach the cracked region through different routes even though some channels are blocked during casting process. Besides, the multiple channels between two nodes also enable multiple healing processes even when some channels are blocked during the previous healing process. In addition, the designed vascular network helps increase the ductility of concrete by increasing crack tortuosity. The schematic figure of a periodic unit-cell is shown in Fig. 1(a). In particular, D, d and t refer to the outer diameter, inner diameter and thickness of vascular respectively. The geometric parameters are listed in Table 1. The vascular network consists of 4 unit cells (Fig. 1(b)).

To investigate the influence of two main printing parameters, i.e., printing layer-height and printing direction (Fig. 2), four sets of vascular network are printed with Acrylonitrile Butadiene Styrene (ABS) filament using a commercial 3D printer Ultimaker 2 +. ABS filament is widely used in 3D printing for its good interlayer adhesion and high chemical resistance. The printing parameters of the four

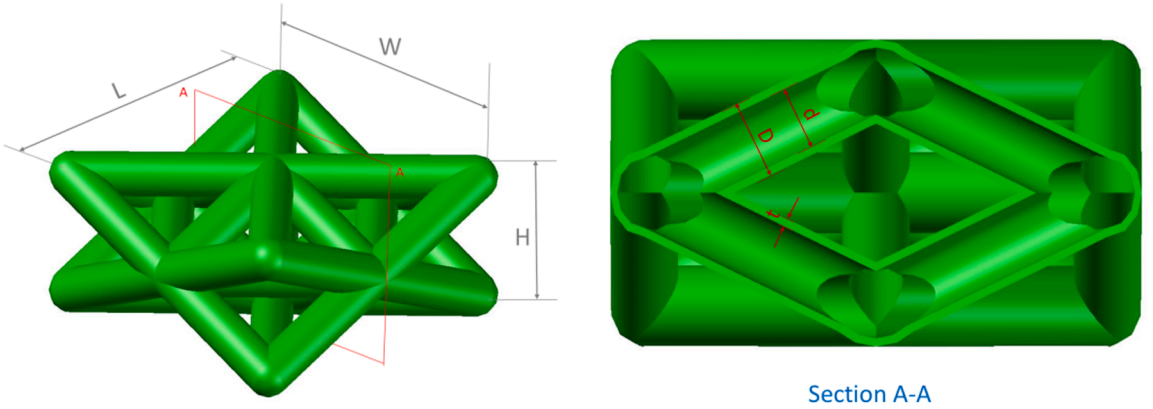

Fig. 1. Schematic figures of vascular network.

Table 1
Geometric parameters of the periodic unit-cell (mm).

Parameter	L	W	H	D	d	t
Value	34	34	14	5	4	0.5

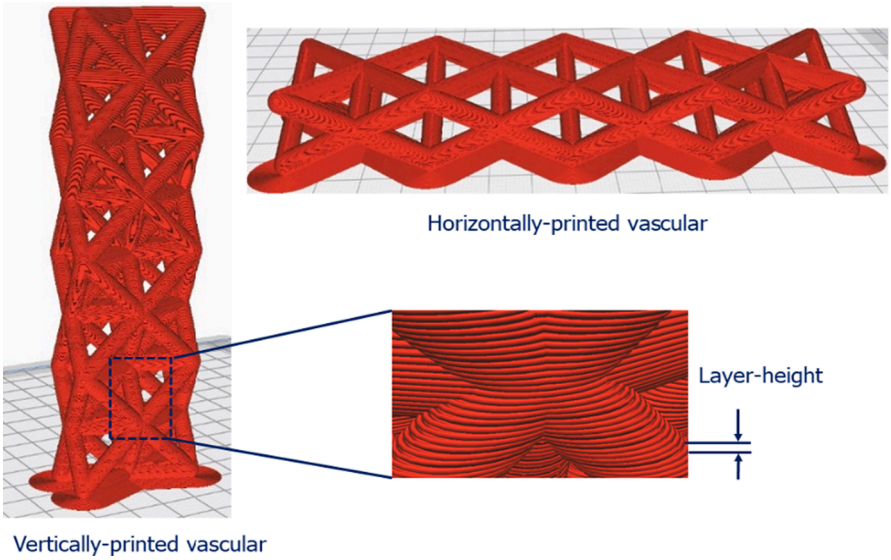

Fig. 2. Schematic showing the influence of printing direction on the 3D-printed vascular network.

ABS vascular are listed in Table 2.

2.2. Casting, curing and healing process

In this study, the matrix mixture uses ordinary Portland cement (CEM I) blended with fly ash, which results in good workability needed to fill the spaces between the tubes of the vascular. In addition, fly ash may also help increase the healing capacity of the matrix for the continuous hydration in the late-age stage [29–31]. The mix proportions are taken from [32] and are listed in Table 3. It should be noted that no additional reinforcement was added in the matrix except the ABS vascular networks. Except the four vascular self-healing concretes, a plain cementitious mortar (i.e. without the vascular) is employed as the reference in the study.

The casting process was as follows: (1) the vascular network was positioned in the foam molds; (2) cement, fly ash and sand were dry-mixed for 4 min in a Hobart blender. (3) superplasticizer and water were added to the dry components and then mixed for 4 min; (4) The mixed materials were poured in the foam molds with a dimension of 160 mm × 40 mm × 25 mm and vibrated for 30 s; (5) The specimens were covered by a plastic film to prevent water evaporation and kept in room temperature for 24 h; (6) The specimens were demolded and cured in a curing chamber (96%±2%RH, 20 ± 2℃) for 27 days before the first round of mechanical tests.

When specimens cracked after the 4-point bending tests, epoxy resin was used as the healing agent for its favorable healing performance [33–35]. Specifically, epoxy resin and hardener were first weighted and mixed with a mass ratio of 3:1 and stirred for 1 min. Then, epoxy resin was manually injected into the vascular networks from one inlet using a syringe. It is noted that the healing agent is not pressurized into the sample. In other words, the epoxy resin flows into the cracks only under gravity and capillary pressure. The amount of epoxy resin is chosen as 5 ml since it ensures that the epoxy resin is enough to reach the crack regions in the experiments. The schematics of the manual healing process is shown in Fig. 3. The treated samples were kept in room temperature for 24 h untill the injected epoxy resin was fully hardened. There are three samples in each group.

Table 2
Main printing parameters of four vascular networks.

	L1H	L1V	L3H	L3V
Layer-height (mm)	0.1	0.1	0.3	0.3
Printing direction	horizontal	vertical	horizontal	vertical
Temperature (℃)	250			
Nozzle size(mm)	0.4			

Table 3
Mix design of the matrix (kg/m^3).

CEM I 42.5 N	Fly ash	Sand (0.125–0.250 mm)	Superplasticizer (Glenium 51)	Water
550	650	550	2	395

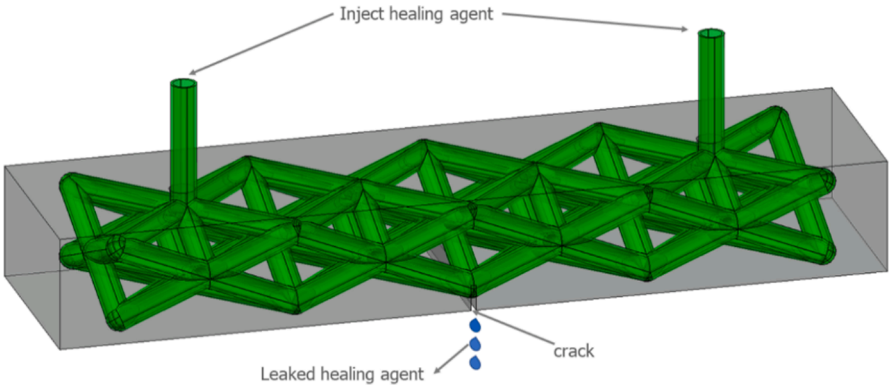

Fig. 3. Schematics of manual healing process.

2.3. Characterization methods

2.3.1. 4-point bending test

Four-point bending tests were carried out by a servo hydraulic press (INSTRON 8872) to evaluate the initial flexural strength and strength regain of the ABS-printed vascular based self-healing concrete. The specimens were loaded with crack opening displacement (COD) control to a predefined maximum crack width. Similar to previous studies [36], the crack opening speed is set to 1 μm/s. The original specimens were loaded until the crack width reached 500 μm. The measurement of crack opening displacement continues to be recorded until the load roller of the hydraulic press does not contact with the tested samples. The crack widths of the specimens after unloading were recorded as the final crack widths. After the healing process, the specimens were loaded again until the the crack width reached 300 μm. The setup of 4-point bending test with two horizontal Linear Variable Differential Transformers (LVDTs) is shown in Fig. 4.

Considering that the deflection of the samples becomes very large and the measurement of the crack width becomes inaccurate when the accumulative crack with reaches 800 μm, only one healing process is carried out when 4-point bending test was controlled by a constant crack opening speed.

To investigate the strength recovery potential for multiple healing process, an additional series of 4-point bending test controlled by a constant vertical displacement speed of 0.01 mm/s was carried out where the specimens were injected epoxy resin for two healing rounds. In each 4-point bending test, the specimens were loaded until the bearing load is less than 0.1KN. The maximum flexural strength in each test was recorded and compared.

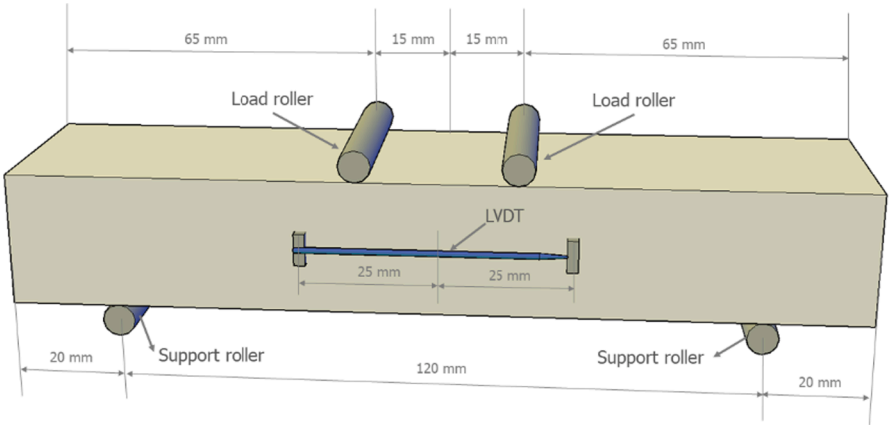

Fig. 4. Four-point bending test setup with horizontal LVDT.

2.3.2. Permeability test

Another problem caused by cracks in concrete is leakage, which may induce corrosion of the reinforcement and shorten the service life. Therefore, permeability is also employed as a metric to evaluate the healing efficiency of the 3D-printed vascular based self-healing concrete.

Considering that the crack width is controlled as 500 μm, the watertightness of the cracked samples was expected to be poor. Therefore, the permeability testing method in [37,38] was used in this study. Particularly, one inlet of the vascular network on the upper surface of samples was sealed by silicone glue while the other was connected to one end of a tube. The other end of the tube was connected to a water container with a water head of 0.5 m from the upper surface of the tested specimens. The schematics of the experimental setup for permeability evaluation is shown in Fig. 5. The steady flow speed of leaked water was automatically recorded and compared to analyze the influence of vascular on the watertightness properties of concrete. The permeability test was carried out before and after injecting epoxy resin.

2.3.3. CT scanning

A micro-CT scanner (Phoenix Nanotom) was used to observe the influence of printing parameters on the printing quality of vascular network. First, the microstructures of hollow bars with 4 different printing parameters (2 printing direction: horizontal and vertical; 2 printing layer-height: 0.1 mm and 0.3 mm) are observed. The microstructures were reconstructed by using the dedicated Phoenix Dotos software. The resolution of the obtained slice for hollow tubes is 3 μm. Besides, the hardened samples embedded with 4 vascular networks were scanned to observe the inner structure of vascular network and the resolution is 27.5 μm.

3. Numerical simulation

3.1. Concrete damaged plasticity model

Numerical simulation is a good alternative to experiments. Compared with experiments, numerical simulation could save time as well as resources. To facilitate the designing of vascular network with ML, numerical simulation is carried out. The simulated results are analyzed and compared with the experimental results. If the simulated results are in agreement with the experimental ones, we could use numerical simulation, rather than lots of experiments to generate dataset for the vascular optimization with ML.

The commercial simulation software Abaqus was employed to simulate the 4-point bending test on the pristine specimens. Concrete damaged plasticity model (CDPM) is often used to study the nonlinear response of cementitious material for its capacity of capturing the main features of the response of concrete [39]. Tension stiffening and compression hardening are defined in Fig. 6. The stress–strain relations under uniaxial tension and compression loading are shown in Equation (1) and (2), respectively.

$$\sigma_t = (1 - d_t)E_0(\varepsilon_t - \widetilde{\varepsilon}_t^{pl}) \tag{1}$$

$$\sigma_c = (1 - d_c)E_0(\varepsilon_c - \widetilde{\varepsilon}_c^{pl}) \tag{2}$$

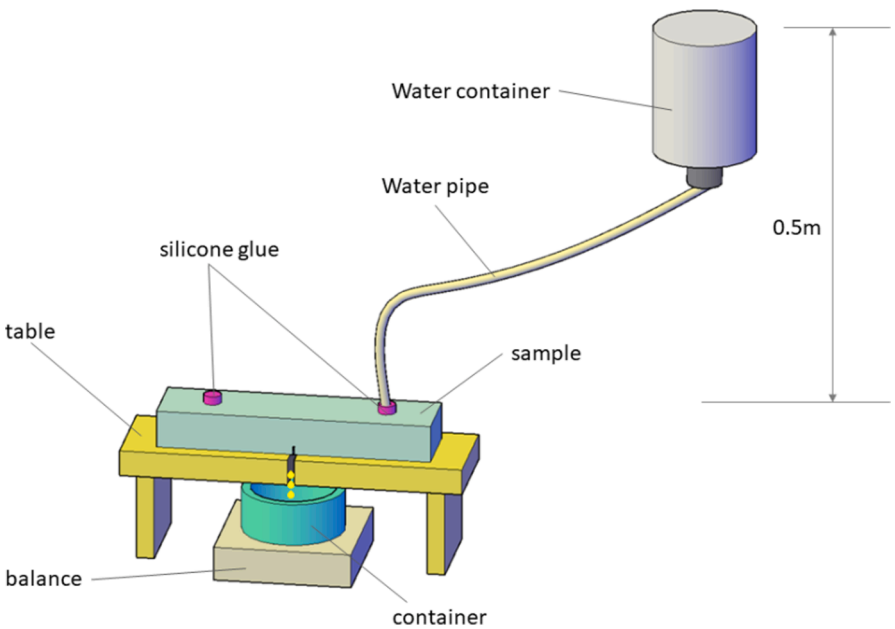

Fig. 5. Schematics of permeability test setup.

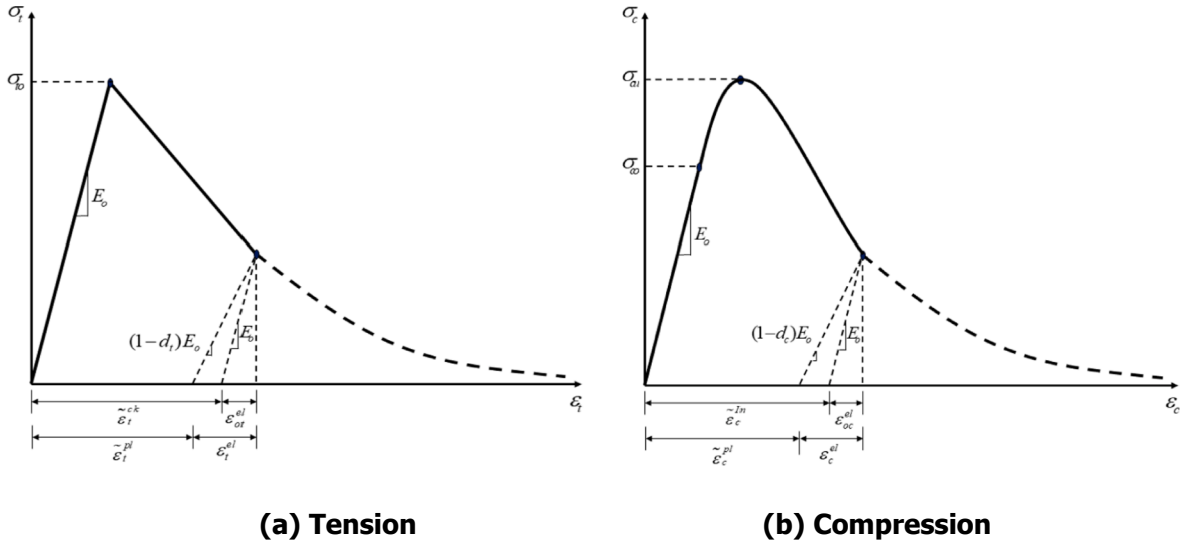

Fig. 6. Constitutive law of CDPM in (a) Tension; (b) Compression.

Whereσ_t, σ_c are the tensile stress and compressive stress respectively;d_t,d_c are tensile damage variable and compressive damage variable ranging from 0 (undamaged) to 1 (total loss of strength). E_0 is the initial (undamaged) elastic stiffness of the material;ε_t, ε_c are the total strains;$\tilde{\varepsilon}_t^{pl}$, $\tilde{\varepsilon}_c^{pl}$ are the equivalent plastic strains. In this study, the stiffness degradation is not considered and the damage variables are set to 0. The equivalent plastic strains are equal to crack strains. As shown in Fig. 6, the crack strains ($\tilde{\varepsilon}_t^{ck}$, $\tilde{\varepsilon}_c^{ck}$) are defined as the total strain minus the elastic strain corresponding to the undamaged materials (Eqs. (3) and (4)).

$$\tilde{\varepsilon}_t^{ck} = \varepsilon_t - \varepsilon_{0t}^{el} \text{ or } \tilde{\varepsilon}_c^{ck} = \varepsilon_c - \varepsilon_{0c}^{el} \tag{3}$$

$$\varepsilon_t^{el} = \sigma_t / E_0 \text{ or } \varepsilon_c^{el} = \sigma_c / E_0 \tag{4}$$

3.2. Model calibration

3.2.1. Calibration for cementitious matrix

Before the numerical simulation, calibration is first carried out to obtain the inputs for models. Because the mix design of cementitious matrix is identical with [32], the input of CDPM for cementitious material is based on the experimental results in the referred article and the fitted result is listed in Table 4.

3.2.2. Calibration for ABS vascular network

According to a previous study [40], 3D-printed ABS shows anisotropic fracture behavior. Therefore, ABS bars with different printing parameters were printed and tested for model calibration. The section of ABS bar is fabricated as small as possible to minimize the size effect caused by 3D printing [41]. Compared to the horizontally-printed ABS bar, the vertical-printed ABS with same section have lower printing quality due to the shorter time interval for cooling. Using a trial and error approach, the section of horizontally- and vertically- printed ABS bars are chosen as 2 mm*1mm and 4 mm*4mm, respectively. The dimension of ABS bars for calibration is listed in Table 5.The Uniaxial tension tests were carried out with a speed of 0.001 mm/s by a Micro Tension-Compression Testing

Table 4
Input parameters for cementitious mortar.

(a) Compressive parameters of cementitious mortar	
Yield stress (MPa)	Inelastic strain(%)
32	0
37	0.149
3	0.18
1	0.20
(b) Tensile parameters of cementitious mortar	
Yield stress (MPa)	Cracking strain(%)
5.8	0
0.1	0.05

Table 5
Dimension of the ABS bars for calibration.

Printing parameters	L1H	L1V	L3H	L3V
Section (mm)	2*1	4*4	2*1	4*4
Length (mm)		40		

device (Fig. 7) and three ABS bars of each group were tested.

The brittle cracking model in Abaus is accurate when the brittle behavior dominates. Therefore, the brittle cracking model in Abaus is employed to define the mechanical response of ABS vascular network during 4-point bending test. The brittle cracking model is used with the linear elastic material model, which define the behavior before cracking. The postfailure stress–strain curve is shown in Fig. 8. σ_t^I is the remaining direct stress after cracking and ϵ_{nn}^{ck} is the direct cracking strain [42].

Considering that the size of the 3D-printed ABS bars were very small, the measured displacements were much higher than the real value due to the defomation of the loading and transmission [43]. Therefore, the measured stresses were directly used as stress inputs while only 1/10 of the measured cracked strains were used as the strain inputs. The input parameters for the 4 kinds of ABS bars are shown in Table 6.

3.3. Interaction setting between vascular network and cementitious matrix

The 6 displacements of the load rollers in the bottom (support) are fixed. The load rollers in the top are loaded downward to 2 mm, while other five displacements are fixed. The 4 load rollers contact with the samples with the contact type of surface-to-surface contact (Explicit), where normal behavior is defined as "hard" contact and tangential behavior if penalty friction with a coefficient of 0.05. The connection between vascular network and cementitious matrix is simplified with tie constraint to accelerate the computing time.

4. Results and discussion

4.1. Fracure behavior of the composites

4.1.1. Flexural response of the vascular based self-healing concretes

Fracture behavior is crucial for self-healing material. Therefore, the ability of the proposed numerical model to simulate the fracture behavior is evaluated. The stress-crack width (CMOD) curves of 4 different specimens are compared with the references (specimens without vascular networks). The experimental and simulated results of specimens under 4-point bending test are shown in Fig. 9. In general, the simulated curves show good agreements with the experimental curves. For all 4 different designs, after the first cracking, a hardening branch can be observed from both experiment and simulations. The extent of this hardening branch is dependent on the printing parameters, although nominally all vascular designs are identical.

It is noted that the flexural strengths of vascular based self-healing concretes are lower than that of the reference, showing that the embedded vascular networks reduce the flexural strength. For the specimens with ABS vascular network, flexural strength of horizontally-printed vascular based self-healing concrete is higher than that of vertically-printed counterparts when the printing layer-height is equal. A possible reason is that the tensile strength of the interlayer between printing layers is poor [43]. When the loading

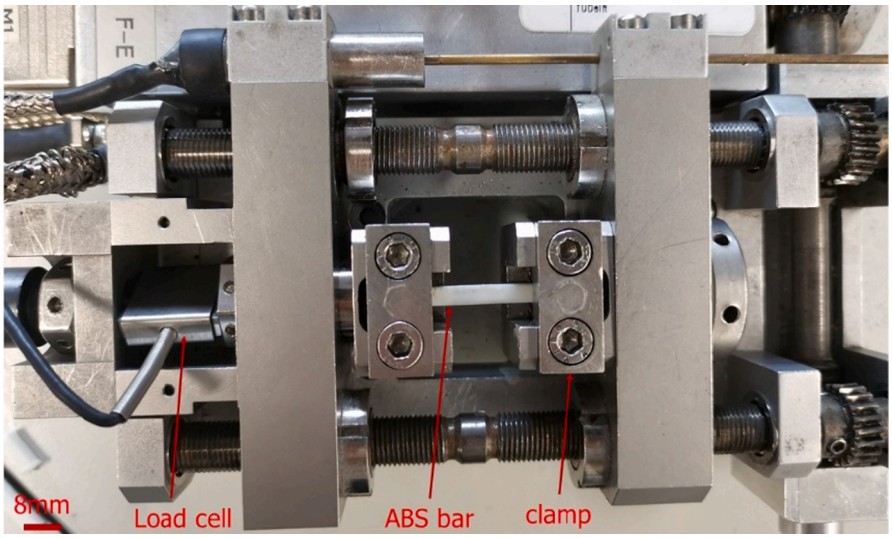

Fig. 7. Micro Tension-Compression Testing device during testing of 3D printed ABS bars.

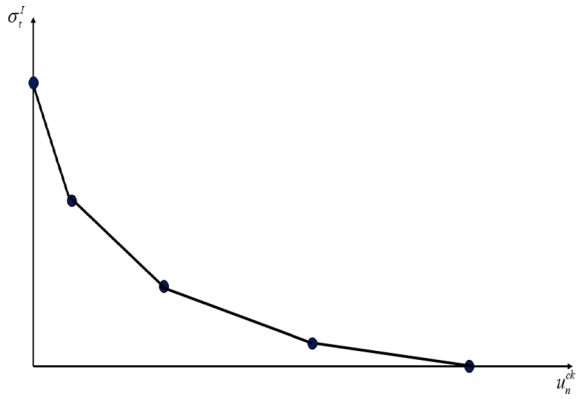

Fig. 8. Postfailure stress–strain curve of ABS (details depend on the printing parameters, see Table 5).

Table 6
Input parameters for ABS vascular.

(a) L1H	
Direct stress after cracking	Direct cracking strain(%)
36.17	0
31.00	0.12
12.01	0.16
0.05	0.29
(b) L3H	
Direct stress after cracking	Direct cracking strain(%)
36.00	0
30.05	0.11
24.00	0.13
0.05	0.20
(c) L1V	
Direct stress after cracking	Direct cracking strain (%)
19.50	0
16.16	0.025
0.11	0.034
0.05	0.075
(d) L3V	
Direct stress after cracking	Direct cracking strain(%)
13.51	0
0.68	0.02
0.05	0.05

direction is perpendicular to the printing direction of vascular networks, the maximum bearing load of the specimens tends to be lower compared with the scenario when the loading direction and the printing direction are same. As to the influence of printing layer-height, flexural strength of the specimens with smaller printing layer-height (0.1 mm) is higher than that of the larger ones (0.3 mm), which agrees with what was expected. In other words, vascular networks with smaller printing layer-height have higher interlayer strength than the those with larger printing layer-height, which would contribute to higher flexural strength.

The curves show different trends after reaching the maximum stress. When the printing direction is horizontal, the stresses remains high level (over 2.0 MPa) till the crack with is over 300 μm. L1H experiences a sudden drop from the second peak to 2.5 MPa when crack width reaches 150 μm, after which the stress stabilizes until droping again when the width is over 300 μm. However, the curve of L3H steadily drops after the second peak and the stress is larger than 2 MPa when the crack width is smaller than 250 μm. When the printing direction is vertical, the curves both witness a steady drop after the second peak. The curve of L3V drops more quickly compared with L1V.

Although the embedded vascular networks do reduce flexural strength, the ductility of ABS-printed vascular based self-healing concretes is higher compared with the references since the ABS vascular acts as the reinforcement for the specimens. The area below the experimental curves is defined as the toughness. For the vascular based self-healing concretes, the toughness is calculated by the area till the crack width is 500 μm, while the reference is calculated till the crack width is 150 μm where the stress is less than 0.1

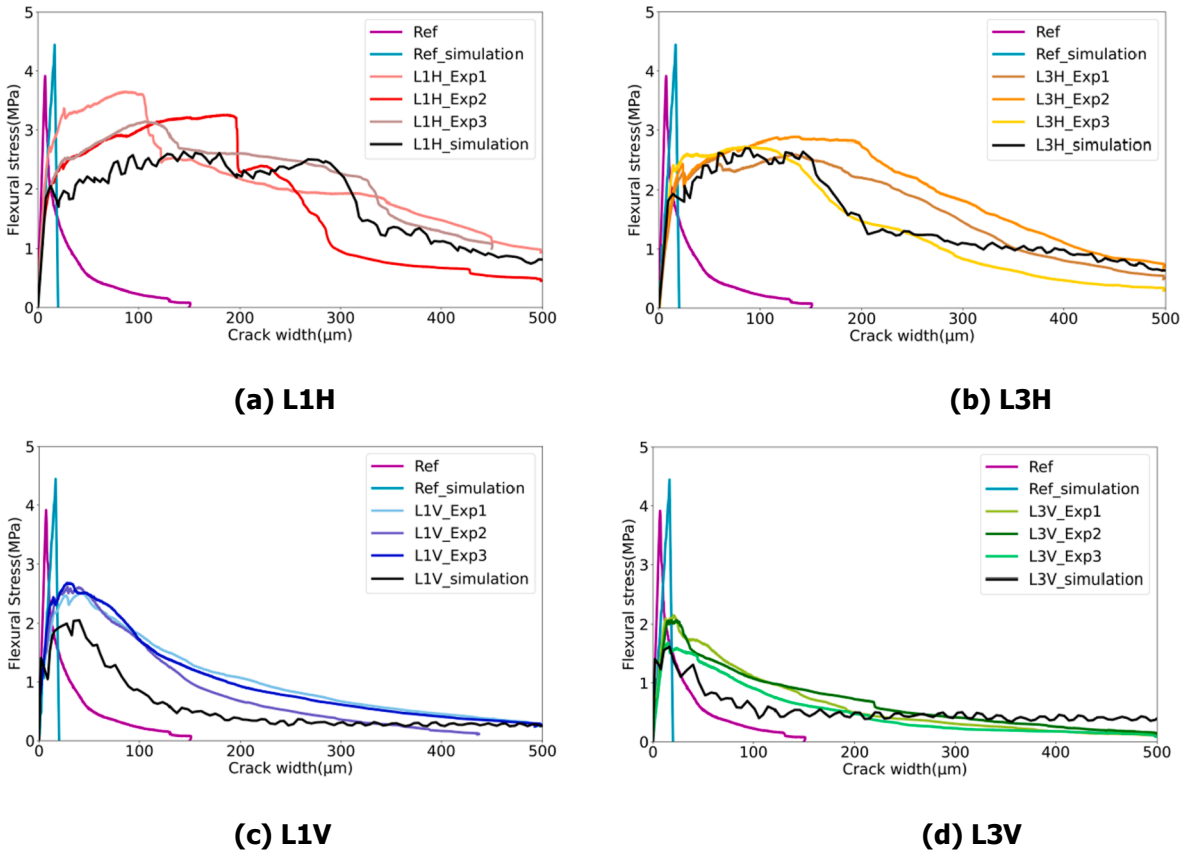

Fig. 9. Flexural response comparison of specimens with different vascular networks.

MPa. Compare with the vascular based self-healing concrete, the reference is brittle and it breaks into two halves when crack width reached 150 μm. The result is shown in Fig. 10.

As shown in Fig. 10, the toughness calculated by numerical simulation is very close to the experimental results, except for L1V. Compared with the reference, the vascular based self-healing concretes absorb more energy. More importantly, it is obvious that the specimens embedded with horizontally printed vascular networks have much higher toughness than the vertically printed counterparts. It is inferred that the horizontally-printed vascular network makes the cracks more tortuous than the vertically-printed ones due to the better ductility.

4.1.2. Crack morphology comparison between simulation and experiments

Except for the flexural response, the crack morphology obtained by the numerical simulations and the experiments is also compared, and the results are shown in Fig. 11 (take L1V as example). Due to the symmetry of the structure, we only simulate half structure to accelerate the computation. Therefore, the crack From Fig. 11, it is noted that the crack morphologies from numerical

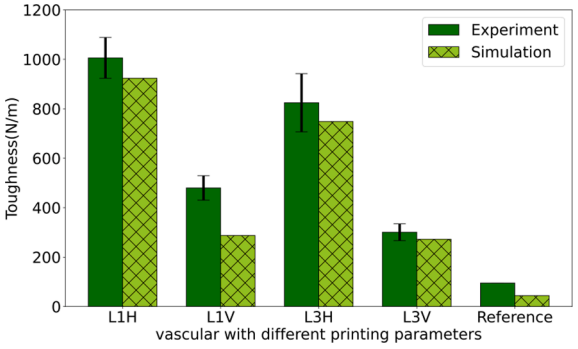

Fig. 10. Toughness comparison of specimens with different vascular networks. (The error bar represents the standard deviation).

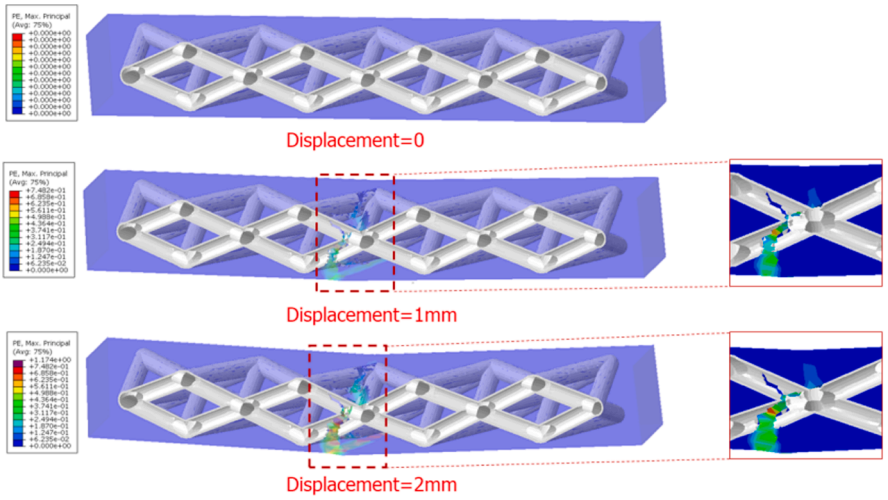

(a) Inner crack evolution from simulation

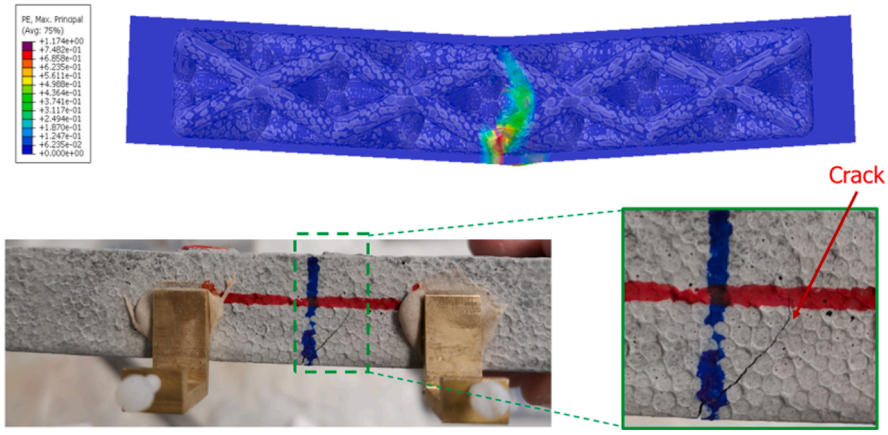

(b) crack morphology from simulation and experiment

Fig. 11. Toughness comparison of specimens with different vascular networks.

simulation and experiment are very similar. There is only one crack from both numerical simulations and experiments and the crack develops upwards with a small angle. The possible reason is that the ABS-printed vascular network is not strong enough to acted as reinforcement that could create multiple cracks. The similar result could be found in [32], where solid octet lattice structures are embedded in cementitious matrix.

4.2. Potential factors influencing simulation accuracy

Although, in general, the simulated results show a good agreement with the experiments, some mismatch still exists. Compared with the experimental results, flexural strengths from numerical simulation are slightly lower than the experimental counterparts for all 4 scenarios. This could be caused by the printing quality of the vascular networks. Therefore, the influence of printing parameters on

Table 7
Printing time and weight of the four kinds of vascular networks.

No.	L1H	L1V	L3H	L3V
Printing time (h)	5	6.5	3	2
Weight (g)	14.75 ± 0.05	13.5 ± 0.2	14.7 ± 0.1	13.5 ± 0.1

the vascular network and the complete self-healing specimens is investigated in this section.

4.2.1. Influence from the microstructure of vascular network

During the printing process, the printing time and the weights of the four vascular networks (3 samples in each group) were measured. The results are given in Table 7.

From Table 7, it is noted that printing time of vascular with a smaller printing layer-height (0.1 mm, L1H and L1V) is much longer than that of a larger printing layer height (0.3 mm, L3H and L3V) as a result of a larger number of printing layers. As to the weight of the vascular network, the printing direction has a significant influence, while the influence of printing layer-height is negligible. The different printing layer-height has significant effect on the roughness of the vascular, which may lower the simulation accuracy.

To investigate the influence of printing parameters on the surface of the vascular, individual hollow ABS bars (D = 5 mm, d = 3 mm) printed using the four different sets of printing parameters were printed. CT scanning was carried out to look into the micro-structure of the vascular. The scanned results are shown in Fig. 12.

From Fig. 12, it can be seen that the interlayer of the vascular printed with a smaller layer-height is much denser than the smaller

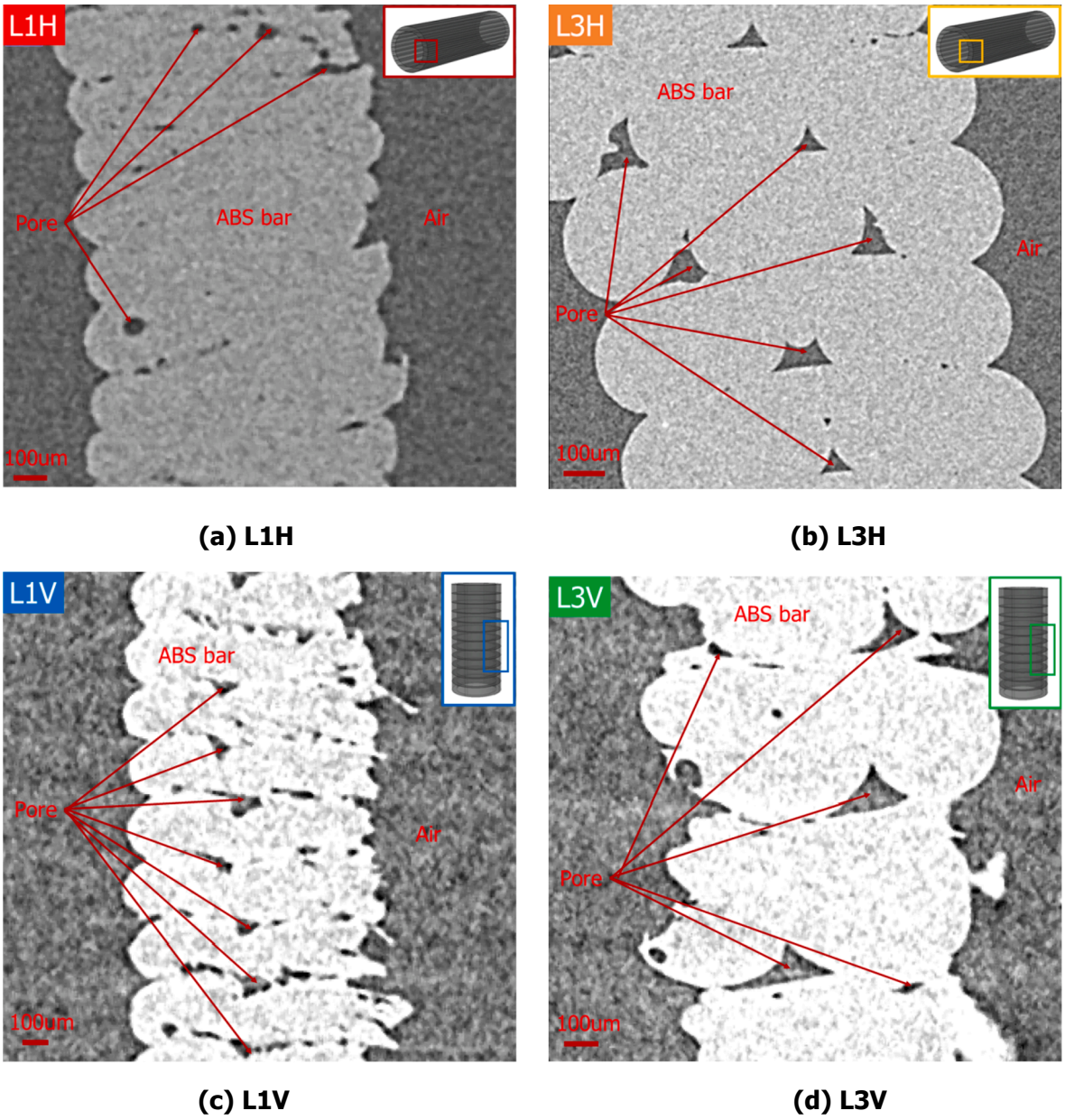

Fig. 12. Printing quality of 3D-printed vascular (a) L1H; (b) L3H; (c) L1V; (d) L3V.

one when the printing direction is the same. The dense interlayer may not only contribute to higher mechanical strength but also help prevent the cementitious matrix from entering the vascular network during casting and causing blockage. When the printing layer-height is the same, there are more pores for the vertically-printed ABS bars. As a result, the flexural strength of the specimens embedded with vertically-printed vascular tends to be lower than the horizontally-printed counterpart.

More importantly, the mechanical interlocking between cementitious matrix and vascular network are different due to the different

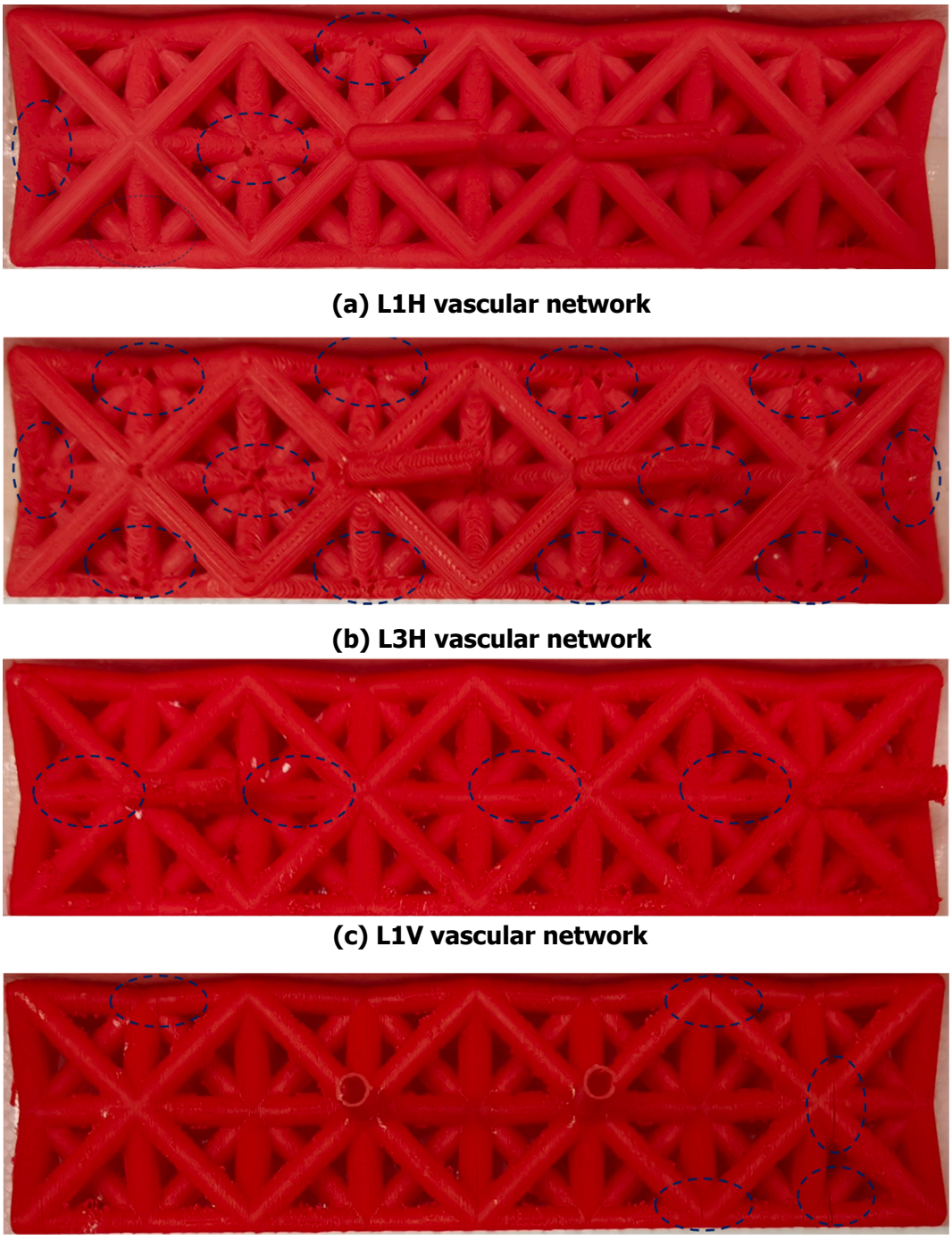

Fig. 13. 3D-printed vascular networks, showing the influence of printing parameters on the printing quality of (large visible pores on the photographed surface are circled): (a) L1H (3 large pores); (b) L3H (12 large pores); (c) L1V (4 large pores); (d) L3V (5 large pores).

roughness of the vascular. Obviously, the surface of the vascular with larger printing layer-height is much rougher than that of the smaller one. However, the different roughness profiles are not considered during numerical simulations since the same interaction type is used for the four scenarios. As a result, the difference between simulated flexural strength and experimental result of the self-healing concretes with larger printing layer-height is narrower than the smaller ones.

4.2.2. *Influence from the macrostructure of vascular network*

Except for ignoring the difference of mechanical interlocking, another factor influencing the simuation accuracy is the overall printing quality of the vascular networks. The printed vascular is shown in Fig. 13.

It can be seen that the vertically-printed vascular networks seem to have better quality than the horizontally-printed ones, as there are some pores in the joint regions for L1H and L3H. Based on the visible defects of the printing vascular, the printing quality of L1V is the best among the four kinds of vascular networks. When the printing direction is horizontal, the printing quality of L3H obviously has much more defects than that of L1H.

The defects in the joint regions may cause leakage of cementitious slurry into the vascular before the cementitious matrix is totally hardened. To verify the inference, CT scanning was carried out to observe the inside of the vascular based self-healing concretes. The resolution of CT scanning is 27.5 μm. If the slurry goes into the L1V vascular, which has the best quality as described above, other vascular networks in self-healing concretes are also likely to be filled with hardened matrix. The scanning results of L1V is shown in Fig. 14.

From Fig. 14, it is obvious that parts of the vascular networks in all cases may be filled with cementitious matrix. However, the numerical simulations do not consider this. As a result, the simulation may underestimate the flexural strength of the vascular based self-healing concretes.

4.3. *Flexural strength recovery*

4.3.1. *Effect of printing parameters on flexural strength recovery*

After the specimens were injected with epoxy resin through the ABS vascular, 4-point bending tests were carried out again to investigate the mechanical recovery. The flexural strengths of the 4 vascular based self-healing concretes before and after the healing process are compared and the results are shown in Fig. 15(a).

To better evaluate the healing capacity of the vascular based self-healing concretes, healing efficiency is employed as a metric. According to the research of Hansen et al [35], healing efficiency of mechanical strength is defined with Equation (5).

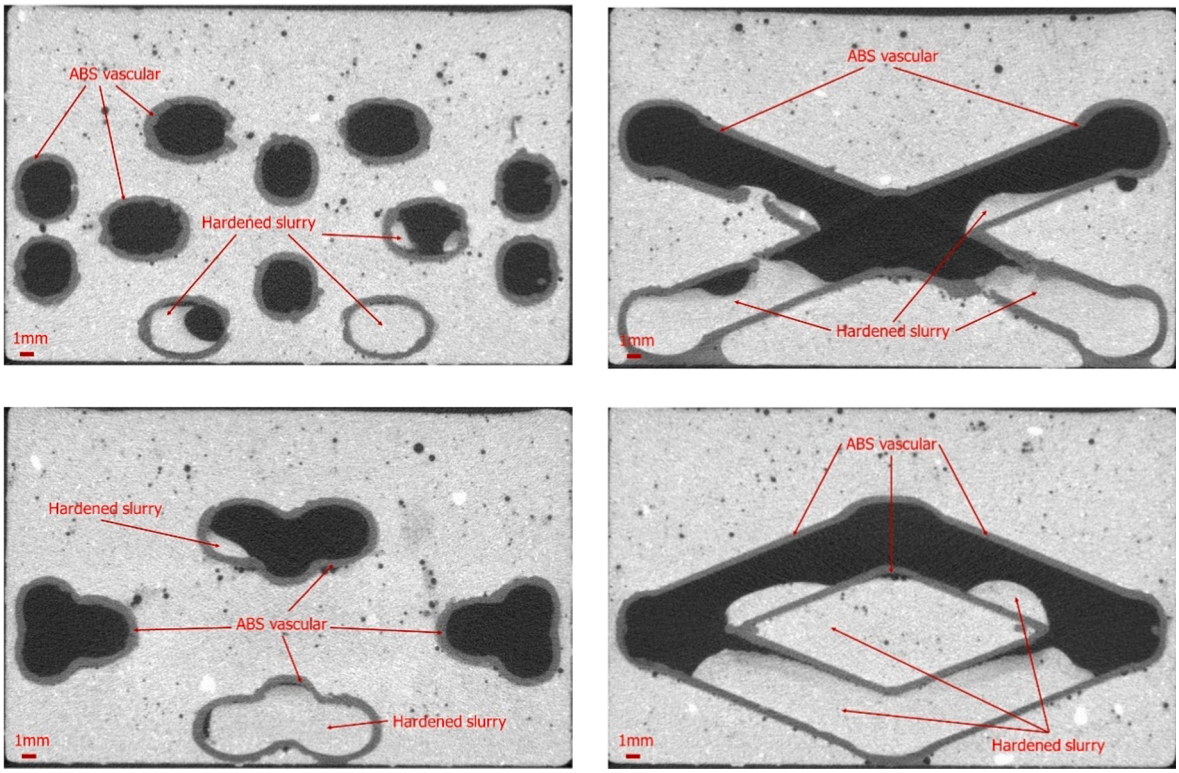

Fig. 14. CT Scanning result of L1V.

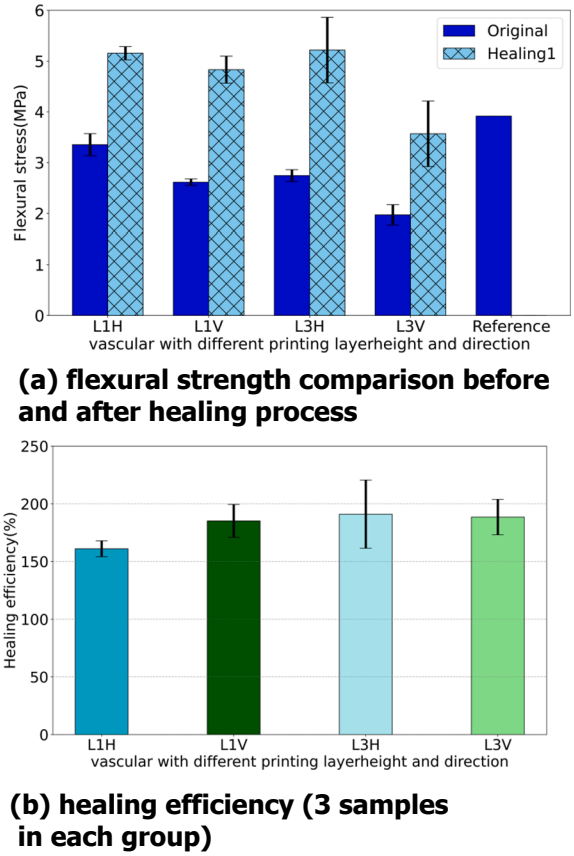

Fig. 15. Healing efficiency of 3D-printed vascular with different printing parameters. (The error bar represents the standard deviation).

$$\eta = \frac{P^{healed}}{P^{original}} \times 100\%. \tag{5}$$

where P^{healed} and $P^{original}$ are the healed fracture load and the original fracture load, respectively.

Based on Eq. (5), the healing efficiency of the vascular based self-healing concrete was calculated and the result is shown in Fig. 15 (b).

From Fig. 15, it is noted that the healing efficiencies of the four ABS-printed vascular based self-healing concretes are all larger than 150%. In other words, the healing efficiency of vascular based self-healing concretes is remarkable when using epoxy resin as the healing agent. Specifically, the average healing efficiency of L3H is the highest among the four scenarios, even though the variation is very large. As to the influence of printing direction on strength regain, the flexural strength of the horizontally-printed vascular specimens is higher than the vertically-printed counterparts after the healing process. The horizontally-printed vascular networks have more defects than the vertically-printed ones. As a result, more slurry enters the vascular and fill part of vascular network. During the healing process, more healing agent was kept in vascular due to the blockage of vascular and it contributes to a higher strength for horizontally-printed vascular self-healing concrete after healing process.

In order to thoroughly study the influence of printing parameters on the mechanical property recovery, the typical mechanical responses of the four vascular based self-healing concretes loaded with a constant crack opening displacement speed before and after the healing process are shown in Fig. 16.

When the crack width of the healed specimen reaches 300 μm, the bearing stress of L1H and L3H are still over 3 MPa while the bearing stress of L1V and L3V are less than 1 MPa, which means that the ductility of horizontally-printed vascular is much better than the vertically-printed ones. It is worth mentioning that the healed fracture strenght of L3V is much lower than the other 3 scenarios (even lower than the strength of the reference). Therefore, vascular network printed with the parameters of L3V has a significant adverse influence on the healing of the specimen. In addition, the areas below the curve for horizontally-printed vascular based self-healing concretes are much larger than the vertically-printed ones, which means that the specimens with horizontally-printed vascular networks absorb more energy during deformation and fracture for the same crack width.

For crack closure after one healing process, the cumulative crack width of horizontally-printed vascular based self-healing concretes (less than 650 μm) is much smaller than the vertically-printed ones (greater than 700 μm). Considering that the healing agent may leak out if the crack width is very large, the horizontally-printed vascular based self-healing concrete seems to have better healing

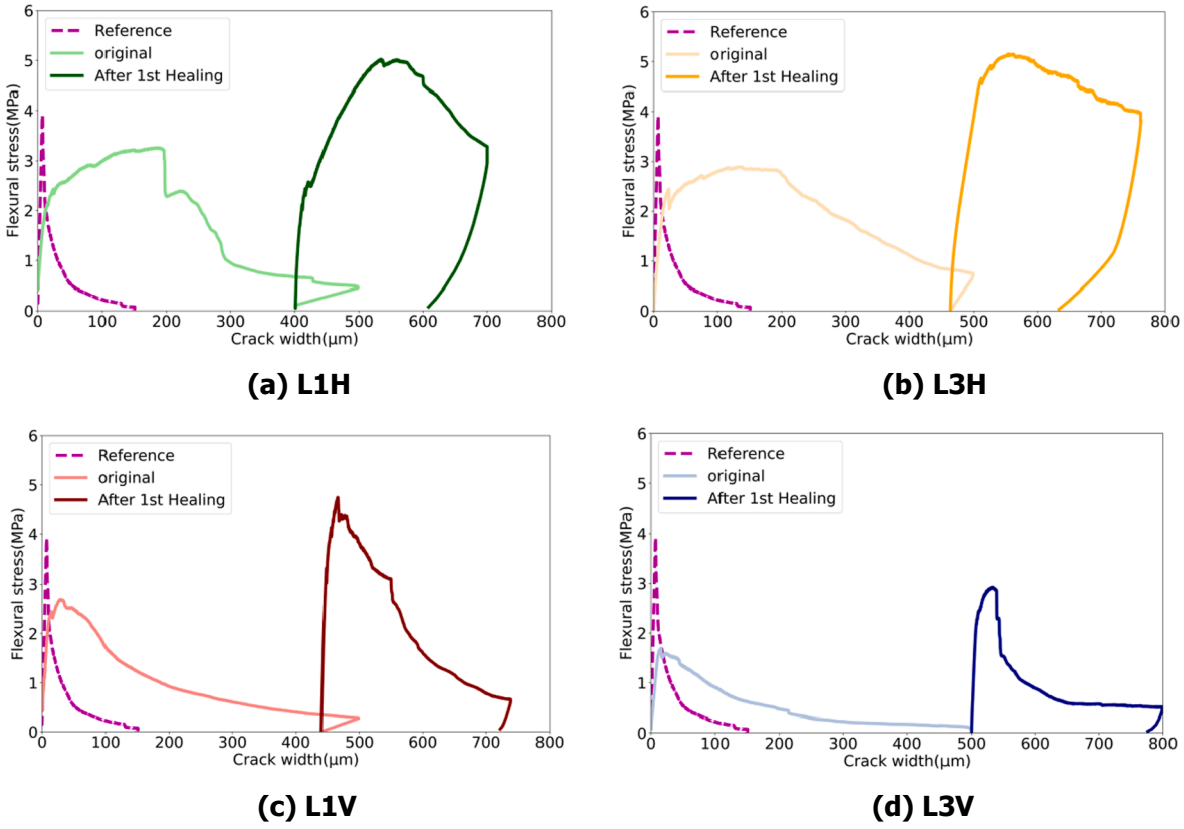

Fig. 16. Flexural stress-crack width curve comparison after the first healing process.

efficiency if an additional round of healing is carried out. According to the experimental results, the crack occurring in the first round of 4-point bending test did not reopen upon reloading. Instead, a different crack developed after the healing process (Fig. 17). Therefore, it can be inferred that the crack in the first 4-point bending test is completely healed during the healing process with epoxy resin as healing agent.

The influence of printing layer-height shows different trends when the printing direction is different. In particular, when the printing direction is horizontal, the flexural strength of vascular-based self-healing concretes does not experience a dramatic change when the printing layer-height increases from 0.1 mm to 0.3 mm. However, the area under the displacement-strength curve of L3H is different from that of L1H, which means that L3H absorbs more energy than L1H during deformation and fracture after one healing process when the crack width reaches 300 μm after the healing process. As for crack closure, unlike the trend after the first 4-point bending test, the crack width of L3H is smaller than that of L1H after the second 4-point bending test. Considering that the first crack is completely healed during the healing process, the actual crack widths of L1H and L3H after the second 4-point bending test are 150 μm and 200 μm, respectively.

When printing direction is vertical, the flexural strength of vascular based self-healing concretes significantly decreases with the increase of printing layer-height, even though the healed fracture stress of L1V and L3V are both higher than the original fracture stress. Compared with L1V, the stress of L3V sharply decreases after it reaches the maximum flexural strength, which means that the absorbed energy is much less than L1V. As to the crack closure, there seems to be no obvious difference of the final crack width between L1V and L3V.

4.3.2. Healing potential of the 4 vascular based self-healing concretes

As mentioned above, the measurement of crack width becomes inaccurate when the deflection reaches 800 μm after the first healing process. In order to investigate the healing potential of these ABS-printed vascular based self-healing concrete, 12 vascular based self-healing concretes were cast and tested in another series of 4-point bending tests. The test was carried out with a constant vertical displacement speed of 0.01 mm/s. The flexural strengths of the specimens after 2 healing processes are compared and the results is shown in Fig. 18.

From Fig. 18, it can be seen that the flexural strengths of horizontally-printed vascular based self-healing concretes are higher than the vertically-printed counterparts. The influence of printing direction on the mechanical strength recovery remains obvious after the second healing process. In addition, it is worth mentioning that the average flexural strength (out of 3 samples) of L3H is the highest after the first/second healing process.

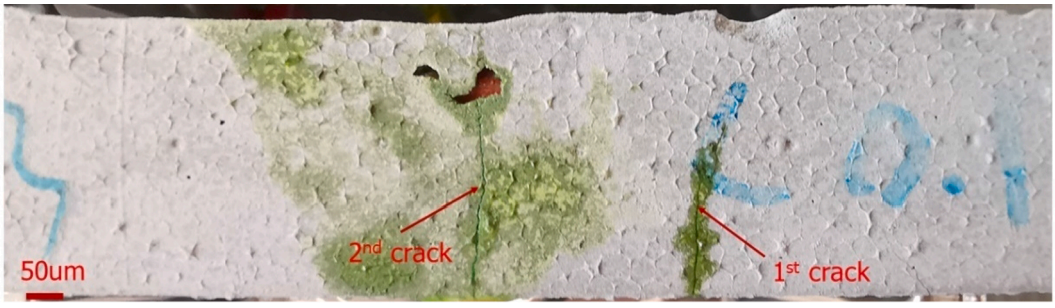

(a) L1H

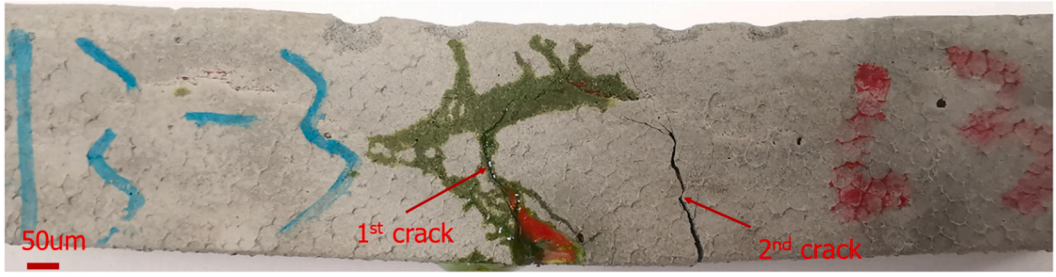

(b) L3H

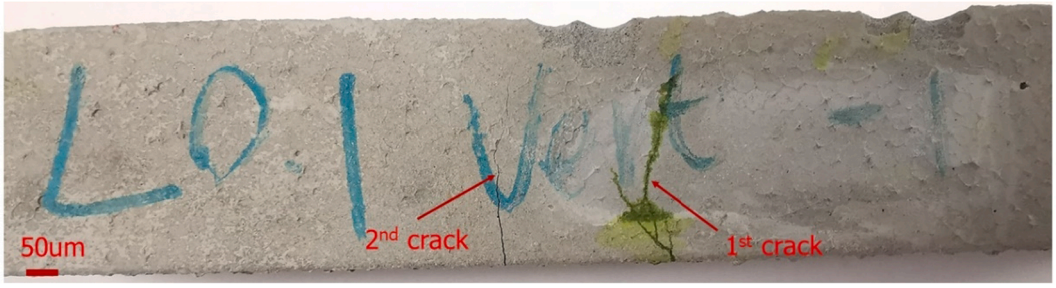

(c) L1V

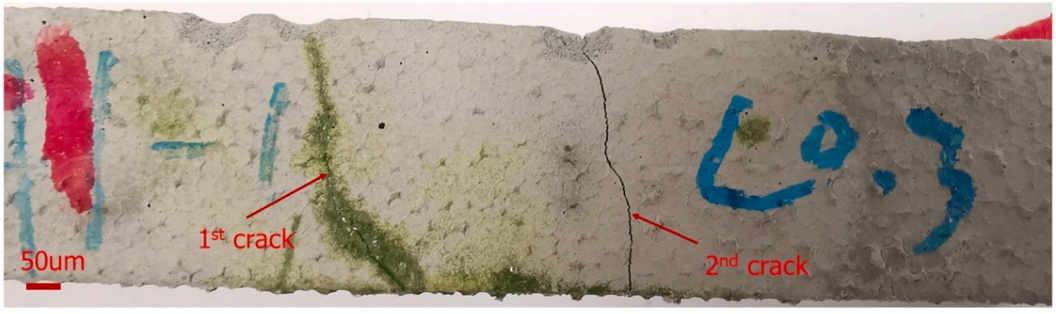

(d) L3V

Fig. 17. Crack morphology after the second 4-point bending test (a) L1H; (b) L3H; (c) L1V; (d) L3V.

Whether the printing direction is horizontal or vertical, specimens with larger printing layer-height (0.3 mm, L3H and L3V) have higher flexural strength than those with smaller printing layer-height (0.1 mm, L1H and L1V) after injecting epoxy resin. However, the difference between them decreases after the second healing process. In other words, the influence of printing layer-height diminishes when 2 healing processes are carried out because an increasing percentage of vascular being filled with epoxy resin.

4.4. Watertightness recovery

Except for the mechanical properties, the influence of printing parameters on watertightness recovery of the 4 vascular based self-

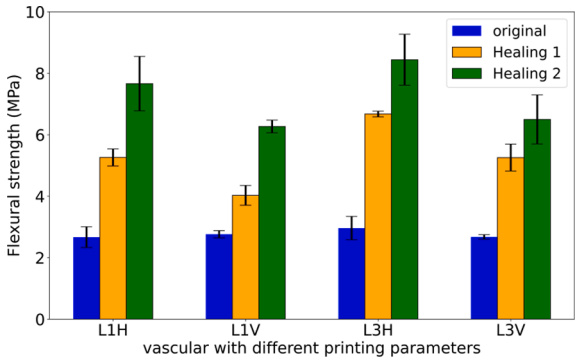

Fig. 18. Flexural strength comparison of specimens (Controlled with constant vertical displacement). (The error bar represents the standard deviation).

healing concretes are also investigated in this study.

4.4.1. *Effect of printing parameters on watertightness recovery*

The crack water permeability test was carried out on cracked specimens before the self-healing procedure to evaluate the influence of printing direction and printing layer-height on the initial permeability of the concretes. There are three samples in each group. The result is shown in Fig. 19.

As presented in Fig. 19, specimens embedded with vertically-printed ABS vascular have poorer watertightness than that of the horizontally-printed ones. Considering that the permeability is related to the crack width of the specimens to the third power, the final crack widths of 4 vascular based self-healing concretes are recorded during the 4-point bending test. The result is shown in Fig. 20. It is noted that the final crack width of horizontally-printed vascular is smaller than that of the vertically-printed ones when printing layer-height is same.

When analyzing the influence of printing layer-height, the results of horizontally-printed vascular and vertically-printed vascular based self-healing concrete show different trends. If only considering the influence of crack closure, vascular networks with larger printing layer-height are expected to have poorer permeability than that of vascular with smaller printing layer-height. However, L3H has a better permeability than L1H, whose final crack width (418 μm) is smaller than L3H (486 μm). One possible reason is that the printing quality of L3H is poorer than that of other vascular, especially in the joint areas. As a consequence, part of the cementitious slurry flows into the vascular during the casting process and blocks part of the vascular network. This inference was verified by the printing quality assessment of 3D-printed vascular provided in Section 4.2.2.

4.4.2. *Effect of printing parameters on watertightness recovery*

After healing the cracks with epoxy resin, permeability tests were carried out to evaluate the watertightness recovery. Similar to [36], the recovery of watertightness is defined in Equation (6):

$$RWT = \frac{W_{n-h}(t) - W_h(t)}{W_{n-h}(t)} \times 100\%. \tag{6}$$

where $W_{n-h}(t)$ and $W_h(t)$ are the average amount of water that has passed through the unhealed and healed cracks of the specimens per second (units in g/s).

The amounts of leaked water through the healed cracks of all 4 kinds of vascular-based self-healing concretes are 0. In other words,

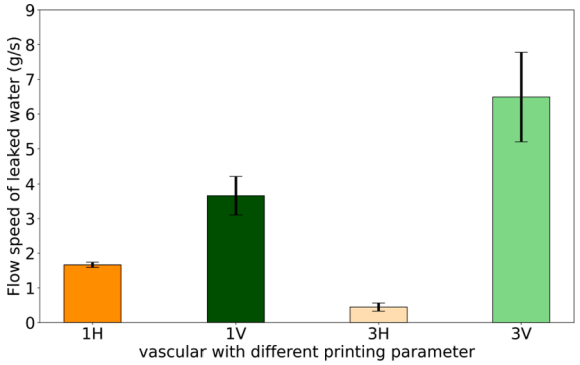

Fig. 19. Flow speed of leaked water of specimens with different vascular networks. (The error bar represents the standard deviation).

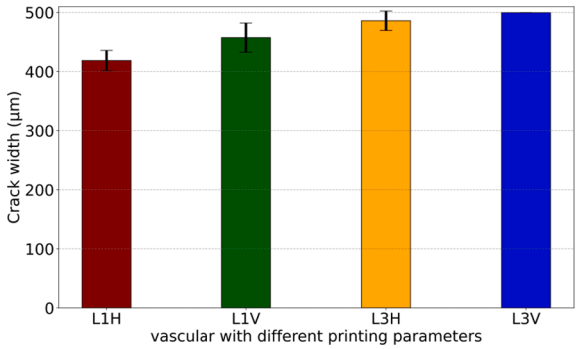

Fig. 20. Final crack widths of specimens with different vascular networks. (The error bar represents the standard deviation).

the watertightness of all investigated vascular based self-healing concretes is fully recovered (i.e. RWT = 100%). The possible reason is that the permeability setup used is only with a water head of 0.5 m and it is hard to measure the flow speed of water. Therefore, in this work, the printing direction and printing layer-height seem to have no obvious influence on the watertightness recovery when using epoxy resin as the healing agent. Further investigation will be carried out in the future.

5. Conclusions

In this work, the influence of printing parameters on the initial properties as well as the healing efficiency of vascular based self-healing concrete was investigated. Vascular networks of the theoretically same geometry were printed with 2 different printing directions and 2 different printing layer-heights. 4-point bending tests were carried out to evaluate the influence on the initial mechanical property and mechanical property recovery. In parallel, numerical simulations were carried out to investigate the feasibility of using CDPM to model the 3D-printed vascular self-healing concrete. In addition, the permeability of the 4 vascular based self-healing concretes before and after healing process were compared. Based on the presented results, the following conclusions can be drawn:

(1) The proposed numerical approach can provide accurate simulation on the fracture behavior of cementitious composites with 3D printed vascular networks. Even with vascular prepared with various printing parameters, the simulated stress-crack with by the Concrete Damaged Plasticity model (CDPM) in Abaqus has shown excellent agreement with experimental results, in terms of crack width and flexural strength under four-point bending. This indicates that the numerical approach has great potential to generate a large mount of data for data-driven design process of the 3D vascular systems.
(2) The printing quality of the vascular networks is identified as a potential factor that may affect the simulation accuracy: The surface roughness difference of the four vascular networks is not considered in simulation, which may lower the simulation accuracy; the defects especially in joint regions cause the leakage of slurry into vascular, leading to an underestimation of results when simulating the 4-point bending test.
(3) Compared with the reference mortar, the vascular-based self-healing cementitious composites have lower initial flexural strength. The specimens with horizontally-printed vascular have higher flexural strength than the vertically-printed counterpart. Vascular networks with smaller printing layer-height has less influence on the initial flexural strength of vascular-based self-healing concrete.
(4) The composites also show good self-healing properties: when using epoxy resin as the healing agent, healing efficiencies in terms of strength regain for the 4 vascular based self-healing concretes are all over 150%, indicating that the flexural strength of the specimens after the healing process is much larger than the original flexural strength. The healing efficiency of L3H is the highest among the 4 vascular based self-healing concretes.
(5) When the specimens were loaded with a constant vertical displacement speed after 2 healing processes, horizontally-printed vascular based self-healing concrete had higher flexural strength than the vertically-printed counterparts after two healing processes. However, the influence of printing layer-height decreases as the number of the healing actions increases.
(6) Similar to the fracture behavior, the printing quality may also affect the watertightness: the horizontally-printed vascular based self-healing concretes have lower intitial permeability than that of the vertically-printed ones. However, the influence of printing layer-height is different when the printing direction is different. Among the 4 specimens, L3H has the best watertightness and one possible reason is that the poor printing quality of L3H vascular induces partial block of the vascular network.
(7) The watertightness recoveries of 4 vascular based self-healing concretes are 100%, which means that the printing direction and printing layer-height do not have obvious effect on the watertightness recovery when using epoxy resin as healing agent.

CRediT authorship contribution statement

Zhi Wan: Conceptualization, Data curation, Investigation, Methodology, Writing – original draft, Formal analysis, Writing – review

& editing. **Yading Xu:** Writing – review & editing, Methodology, Investigation, Data curation, Conceptualization. **Yu Zhang:** Writing - review & editing, Data curation, Investigation. **Shan He:** Writing – review & editing, Investigation. **Branko Šavija:** Conceptualization, Supervision, Writing – review & editing.

Declaration of Competing Interest

The authors declare that they have no known competing financial interests or personal relationships that could have appeared to influence the work reported in this paper.

Acknowledgement

Zhi Wan, Yading Xu and Yu Zhang would like to acknowledge the financial support of the China Scholarship Council (CSC) under the grant agreement No.201906220205, No. 201708110187 and No. 201808320456. Branko Šavija would like to acknowledge the financial support of an European Union Horizon 2020 project InnovaConcrete (Innovative Materials and Techniques for the Conservation of 20th Century Concrete-Based Cultural Heritage), Grant Agreement Number 760858. The authors would like to acknowledge Mr. Maiko van Leeuwen and Mr. Arjan Thijssen for their support in mechanical tests and CT scanning tests.

References

[1] Davies RE, Jefferson A, Lark R, Gardner D. A novel 2D vascular network in cementitious materials 2015.
[2] Hilloulin B, Hilloulin D, Grondin F, Loukili A, De Belie N. Mechanical regains due to self-healing in cementitious materials: Experimental measurements and micro-mechanical model. Cem Concr Res 2016;80:21–32. https://doi.org/10.1016/j.cemconres.2015.11.005.
[3] Van Tittelboom K, De Belie N. Self-Healing in Cementitious Materials—A Review. Self-healing in cementitious materials-a review Materials (Basel) 2013;6(6):2182–217.
[4] Blaiszik BJ, Kramer SLB, Olugebefola SC, Moore JS, Sottos NR, White SR. Self-healing polymers and composites. Annu Rev Mater Res 2010;40:179–211. https://doi.org/10.1146/annurev-matsci-070909-104532.
[5] Lee MW, An S, Yoon SS, Yarin AL. Advances in self-healing materials based on vascular networks with mechanical self-repair characteristics. Adv Colloid Interface Sci 2018;252:21–37. https://doi.org/10.1016/j.cis.2017.12.010.
[6] Dry C. Matrix cracking repair and filling using active and passive modes for smart timed release of chemicals from fibers into cement matrices. Smart Mater Struct 1994;3:118–23. https://doi.org/10.1088/0964-1726/3/2/006.
[7] Mihashi H, Kaneko Y, Nishiwaki T, Otsuka K. Fundamental study on development of intelligent concrete characterized by self-healing capability for strength. Trans Japan Concr Inst 2000;22:441–50.
[8] Hamilton AR, Sottos NR, White SR. Self-healing of internal damage in synthetic vascular materials. Adv Mater 2010;22:5159–63. https://doi.org/10.1002/adma.201002561.
[9] Minnebo P, Thierens G, De Valck G, Van Tittelboom K, De Belie N, Van Hemelrijck D, et al. A novel design of autonomously healed concrete: Towards a vascular healing network. Materials (Basel) 2017;10(1):49.
[10] Sangadji S, Schlangen E. Self healing of concrete structures - Novel approach using porous network concrete. J Adv Concr Technol 2012;10:185–94. https://doi.org/10.3151/jact.10.185.
[11] Zhang W, Zheng Q, Ashour A, Han B. Self-healing cement concrete composites for resilient infrastructures: A review. Compos Part B Eng 2020;189:107892. https://doi.org/10.1016/j.compositesb.2020.107892.
[12] Zhu DY, Rong MZ, Zhang MQ. Self-healing polymeric materials based on microencapsulated healing agents: From design to preparation. Prog Polym Sci 2015;49–50:175–220. https://doi.org/10.1016/j.progpolymsci.2015.07.002.
[13] Yerro O, Radojevic V, Radovic I, Petrovic M, Uskokovic PS, Stojanovic DB, et al. Thermoplastic acrylic resin with self-healing properties. Polym Eng Sci 2016;56(3):251–7.
[14] Dry CM. Three designs for the internal release of sealants, adhesives, and waterproofing chemicals into concrete to reduce permeability. Cem Concr Res 2000;30:1969–77. https://doi.org/10.1016/S0008-8846(00)00415-4.
[15] Li VC, Lim YM, Chan YW. Feasibility study of a passive smart self-healing cementitious composite. Compos Part B Eng 1998;29:819–27. https://doi.org/10.1016/S1359-8368(98)00034-1.
[16] Williams HR, Trask RS, Bond IP. Self-healing sandwich panels: Restoration of compressive strength after impact. Compos Sci Technol 2008;68:3171–7. https://doi.org/10.1016/j.compscitech.2008.07.016.
[17] Williams HR, Trask RS, Bond IP. Self-healing composite sandwich structures. Smart Mater Struct 2007;16:1198–207. https://doi.org/10.1088/0964-1726/16/4/031.
[18] Selvarajoo T, Davies RE, Freeman BL, Jefferson AD. Mechanical response of a vascular self-healing cementitious material system under varying loading conditions. Constr Build Mater 2020;254:119245. https://doi.org/10.1016/j.conbuildmat.2020.119245.
[19] Patrick JF, Hart KR, Krull BP, Diesendruck CE, Moore JS, White SR, et al. Continuous self-healing life cycle in vascularized structural composites. Adv Mater 2014;26(25):4302–8.
[20] Boba K, Heath C, Bond IP, Wass DF. Novel Manufacturing Method for FRP Composites With a Multifunctional Vascular Network. 4th Int Conf Self-Healing Mater 2013:388–91.
[21] Toohey KS, Sottos NR, Lewis JA, Moore JS, White SR. Self-healing materials with microvascular networks. Nat Mater 2007;6:581–5. https://doi.org/10.1038/nmat1934.
[22] Li Z, de Souza LR, Litina C, Markaki AE, Al-Tabbaa A. A novel biomimetic design of a 3D vascular structure for self-healing in cementitious materials using Murray's law. Mater Des 2020;190:108572. https://doi.org/10.1016/j.matdes.2020.108572.
[23] Dwiyati ST, Kholil A, Riyadi R, Putra SE. Influence of layer thickness and 3D printing direction on tensile properties of ABS material. J Phys Conf Ser 2019;1402(6):066014. https://doi.org/10.1088/1742-6596/1402/6/066014.
[24] Toohey KS, Sottos NR, Lewis JA, Moore JS, White SR. Self-healing materials with microvascular networks. Nat Mater 2007;6(68):581–5. https://doi.org/10.1038/nmat1934.
[25] Wang K-M, Lorente S, Bejan A. Vascularization with grids of channels: multiple scales, loops and body shapes. J Phys D Appl Phys 2007;40(15):4740–9.
[26] Aragón AM, Wayer JK, Geubelle PH, Goldberg DE, White SR. Design of microvascular flow networks using multi-objective genetic algorithms. Comput Methods Appl Mech Eng 2008;197:4399–410. https://doi.org/10.1016/J.CMA.2008.05.025.
[27] Guo K, Yang Z, Yu C-H, Buehler MJ. Artificial intelligence and machine learning in design of mechanical materials. Mater Horizons 2021;8:1153–72. https://doi.org/10.1039/d0mh01451f.
[28] Chen C-T, Gu GX. Generative Deep Neural Networks for Inverse Materials Design Using Backpropagation and Active Learning. Adv Sci 2020;7:1902607. https://doi.org/10.1002/ADVS.201902607.

[29] Zhou Z, Li Z, Xu D, Yu J. Influence of slag and fly ash on the self-healing ability of concrete. Adv. Mater. Res., vol. 306–307, Trans Tech Publications Ltd; 2011, p. 1020–3. https://doi.org/10.4028/www.scientific.net/AMR.306-307.1020.
[30] Chindasiriphan P, Yokota H, Pimpakan P. Effect of fly ash and superabsorbent polymer on concrete self-healing ability. Constr Build Mater 2020;233:116975. https://doi.org/10.1016/j.conbuildmat.2019.116975.
[31] Termkhajornkit P, Nawa T, Yamashiro Y, Saito T. Self-healing ability of fly ash-cement systems. Cem Concr Compos 2009;31:195–203. https://doi.org/10.1016/j.cemconcomp.2008.12.009.
[32] Xu Y, Zhang H, Gan Y, Šavija B. Cementitious composites reinforced with 3D printed functionally graded polymeric lattice structures: Experiments and modelling. Addit Manuf 2021;39:101887. https://doi.org/10.1016/j.addma.2021.101887.
[33] Hansen CJ, White SR, Sottos NR, Lewis JA. Accelerated self-healing via ternary interpenetrating microvascular networks. Adv Funct Mater 2011;21:4320–6. https://doi.org/10.1002/adfm.201101553.
[34] Norris CJ, Bond IP, Trask RS. The role of embedded bioinspired vasculature on damage formation in self-healing carbon fibre reinforced composites. Compos Part A Appl Sci Manuf 2011;42:639–48. https://doi.org/10.1016/j.compositesa.2011.02.003.
[35] Hansen CJ, Wu W, Toohey KS, Sottos NR, White SR, Lewis JA. Self-healing materials with interpenetrating microvascular networks. Adv Mater 2009;21:4143–7. https://doi.org/10.1002/adma.200900588.
[36] Tziviloglou E, Wiktor V, Jonkers HM, Schlangen E. Bacteria-based self-healing concrete to increase liquid tightness of cracks. Constr Build Mater 2016;122:118–25. https://doi.org/10.1016/j.conbuildmat.2016.06.080.
[37] Tziviloglou E, Pan Z, Jonkers HM, Schlangen E. Bio-based self-healing mortar: An experimental and numerical study. J Adv Concr Technol 2017;15:536–43. https://doi.org/10.3151/jact.15.536.
[38] Gruyaert E, Debbaut B, Snoeck D, Díaz P, Arizo A, Tziviloglou E, et al. Self-healing mortar with pH-sensitive superabsorbent polymers: testing of the sealing efficiency by water flow tests. Smart Mater Struct 2016;25(8):084007. https://doi.org/10.1088/0964-1726/25/8/084007.
[39] Chaudhari SV, Chakrabarti MA. Modeling of Concrete for Nonlinear Analysis using Finite Element Code ABAQUS. Int J Comput Appl 2012;44(7):14–8.
[40] Hart KR, Wetzel ED. Fracture behavior of additively manufactured acrylonitrile butadiene styrene (ABS) materials. Eng Fract Mech 2017;177:1–13. https://doi.org/10.1016/J.ENGFRACMECH.2017.03.028.
[41] Nurizada A, Kirane K. Induced anisotropy in the fracturing behavior of 3D printed parts analyzed by the size effect method. Eng Fract Mech 2020;239:107304. https://doi.org/10.1016/j.engfracmech.2020.107304.
[42] Hillerborg A, Modéer M, Petersson PE. Analysis of crack formation and crack growth in concrete by means of fracture mechanics and finite elements. Cem Concr Res 1976;6:773–81. https://doi.org/10.1016/0008-8846(76)90007-7.
[43] Xu Y, Zhang H, Šavija B, Chaves Figueiredo S, Schlangen E. Deformation and fracture of 3D printed disordered lattice materials: Experiments and modeling. Mater Des 2019;162:143–53. https://doi.org/10.1016/j.matdes.2018.11.047.